Bubble entrapment mechanisms during the impact of a water drop

J.-L. Liow[1] and D.E. Cole[2]

[1]School of Aeronautical, Civil and Mechanical Engineering
UNSW@ADFA, Northcott Drive, ACT, 2600 AUSTRALIA

[2]DEC-MECH PTY. LTD.,
200 Ross River Road, Aitkenvale QLD 4814 AUSTRALIA

Abstract

The formation of bubbles in liquid-liquid impacts was studied with the aid of a high speed video. The resulting mechanisms for the formation of bubbles can be broken into three main groups: bubbles formed on initial drop impact, bubbles formed due to cavity collapse, and bubbles formed from thin film rupture by a floating drop. The largest bubble was formed by cavity collapse while fine clouds of bubbles were formed by a number of different mechanisms. The bubble sizes range from below 12 µm to almost 1 mm in diameter, a range of almost three magnitudes. The regions for the different bubble mechanisms are a function of the Froude and Weber number of the impacting drop. In the region where floating drops exist, bubbles were generally formed from film drainage when We<6, while bubbles formed during rupture of a rapidly expanding trapped air film occurred between 6<We<20.

Introduction

The characteristic pinging sound heard when a drop of water splashes into a pool of water is familiar to most people. Often with the large raindrops, the impact is followed by a large bubble that floats on the water surface for some time before bursting. In the 1950's, Franz [3] showed that rainfall produced a large spectrum of sound frequencies ranging from the audible to 50kHz. Blanchard and Woodcock [1] showed that under certain conditions the impact of a liquid drop can leave many micro-bubbles entrapped in the bulk fluid. Esmailizadeh and Mesler [2] provided the first series of images showing hundred, possibly thousands, of micro-bubbles (< 200 µm) being formed after the impact of a liquid drop. Furthermore, the bubbles were being transported deep into the fluid by a vortex ring. Further investigation by Sigler and Mesler [9] showed that the bubbles originated from the destruction of a thin air film between the drop and pool surface.

Pumphrey and Crum [7] measured the acoustic trace from splashing drops and Oguz and Properetti [6] confirmed that the audible sound from a splashing drop was due to the entrapment of a bubble by the collapsing cavity. Rein [8] showed that the entrapment of the bubble was accompanied by the formation of a high speed jet. Liow [4] showed that the jet formation region occurred over a wider Froude [$Fr=u^2/(gh)$] and Weber [$We=\rho u^2 L/\sigma$] numbers region than the bubble entrapment regime, and that bubbles could be entrapped at higher Fr and We numbers than previously observed. He also noted the presence of small bubbles present in the bulk fluid just ahead of the expanding cavity for low We and Fr number conditions.

Thoroddsen *et al.* [10] observed that a thin air film is trapped between the impacting drop and the bulk fluid. They observed the rupture of the gaseous film at very different stages of cavity development and showed that the film could contract to form two small bubbles (50–200 µm) or shatter to form a cloud of micro-

bubbles (< 15 µm) as seen by Sigler and Mesler [9]. Both Thoroddsen *et al.* [10] and Sigler and Mesler [9] used large drops (4 mm in diameter) that were significantly non-spherical at impact. Whether the shape of the bubble during impact plays an important part in the trapping of bubbles has not been fully explored, and there is no definitive classification of the conditions for the different bubble entrapment cases.

An investigation into the formation of bubbles due to the impact of a water drop on a large bath of water was carried out by varying the drop size and the impact velocity (different height of fall). The mechanisms found for bubble formation or entrapment were classified into three different groups:

1. ***Bubbles formed on initial drop impact***;

- Thoroddsen bubbles - occurs when a disc of air is trapped between the bulk fluid and impacting drop. The disc retracts to form a few large bubbles ranging from 60 to 250 µm in diameter.

- Oguz-Prosperetti bubble rings - occurs when sites of trapped air form into a ring shaped area surrounding the original impact site. The bubbles are smaller than 12 µm in diameter.

2. ***Bubbles formed during cavity collapse***:

- Primary bubble entrapment - usually a large bubble is trapped at the base of the collapsing cavity which vibrates audibly when it is pinched off.

- Secondary bubble entrapment - bubbles formed during the collapse stage of the cavity due to surface instabilities that appear on the lower surface of the cavity base.

3. ***Bubbles formed from thin film rupture with a floating drop***:

- Film thinning and rupture due to drainage - occurs when an impacted drop sits on the bulk fluid and the air film in between slowly drains before shattering.

- Film thinning and rupture due to rapid expansion - occurs when the disc of air between the bulk fluid and impacting drop spreads out thinly before shattering.

Experimental

A Cole-Palmer 74900 Series syringe pump provided the flow to the ends of 33, 26 and 20G flat tipped needles [drops of 2.06±0.060, 2.53 ±0.044, and 3.13±0.044 mm diameter respectively] to provide three different drop sizes. The drop generating device was mounted on a traversing rail where the height could be adjusted from 0 to 700 mm from the bulk liquid free surface with a resolution of 12 µm [4]. A pair of Redlake HG-100K video cameras with a 1000 fps at full frame (1504×1128) or up to 100,000 fps at reduced frame sizes was used to capture the splash event above and below the water line simultaneously. A 105 mm Micro-Nikkor lens, set at f11, with a pixel resolution of 12 µm was used. Lighting was provided with

an Arri Studio 5 kW tungsten-Fresnel lamp. The falling drops cut a laser beam to start the video recording. The images were stored as tiff files and numbered in sequential order on a hard disk drive.

The experimental observations and results will be divided into the three groups listed above.

Bubbles formed from initial drop impact

The bubbles formed in this group of phenomena are from the early stages of the impact of a drop on the bulk fluid. Immediately after impact the drop interacts with the bulk fluid and coalesces without the drop leaving the surface of the bulk fluid again. This occurs at $We>20$. When a drop impacts on the bulk fluid, a film of air is trapped between the drop and the bulk fluid. As the impact progresses, the air is thinned out into a disk.

Thoroddsen bubbles

When the impact Froude number is low, the drop does not have enough kinetic energy to thin the air disk till it shatters. As a result, the air disk is able to contract. As Thoroddsen *et al.* [10] showed, an azimuthal undulation, resembling a pearl necklace, develops along its edges and the air film contracts to a single bubble or it may break up to form two or more smaller air bubbles. The air film dynamics is controlled by a balance of inertia and surface tension forces where the $We\sim1$.
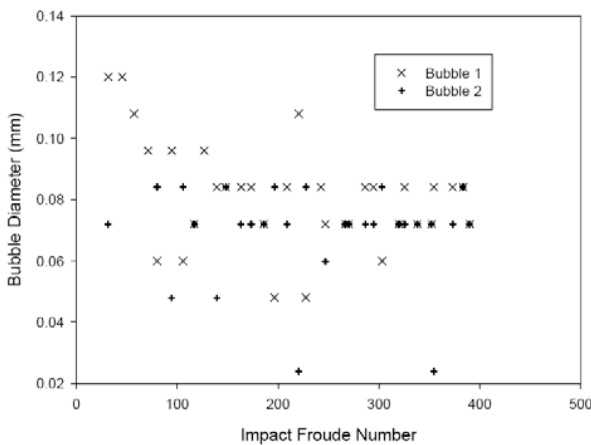

Figure 1. Diameters of Thoroddsen bubbles from the impact of a 3.13 ± 0.04 mm (20G needle) for $30<Fr<400$. Some impacts, usually $Fr<60$, only gave one bubble. Note that the two bubbles formed are often similar in diameter with only a few exceptions where the two bubble diameters differ significantly.

It is interesting to note in Figure 1 that the bubble size is larger at low Fr but rapidly converges to a steady bubble diameter above $Fr>80$. Thus the total air trapped between the impacting drop and bulk fluid is constant ($\sim4.4\times10^{-4}$ mm^3) over a large Fr range. This finding is in contradiction to Thoroddsen *et al.* [10] where the diameter of the disk was constant for a given impact radius of curvature and the thickness decreased with increasing impact Reynolds [$Re=ud/\upsilon$] number (or increasing impact Fr). The result of Thoroddsen *et al.* [9] will result in a smaller bubble as the Fr increases.

Oguz-Prosperetti bubble rings

Oguz and Prosperetti [5] suggested that capillary disturbances formed on the drop surface in the early stages of impact should trap a toroidal quantity of air around the impact site but provided no evidence to support their theory. Thoroddsen *et al.* [9] provided some experimental evidence but did not investigate the phenomena in detail or show any images of the actual interface deformation that leads to the formation of the bubble rings. Due to the small size of the micro-bubbles, it is difficult to resolve their presence. In this investigation, no direct evidence to support

the formation of Oguz-Prosperetti bubble ring was observed. However, some secondary phenomena (Figure 2) that may be the end result of Oguz-Prosperetti bubble ring formation and break-up was observed from the presence of micro-bubbles.
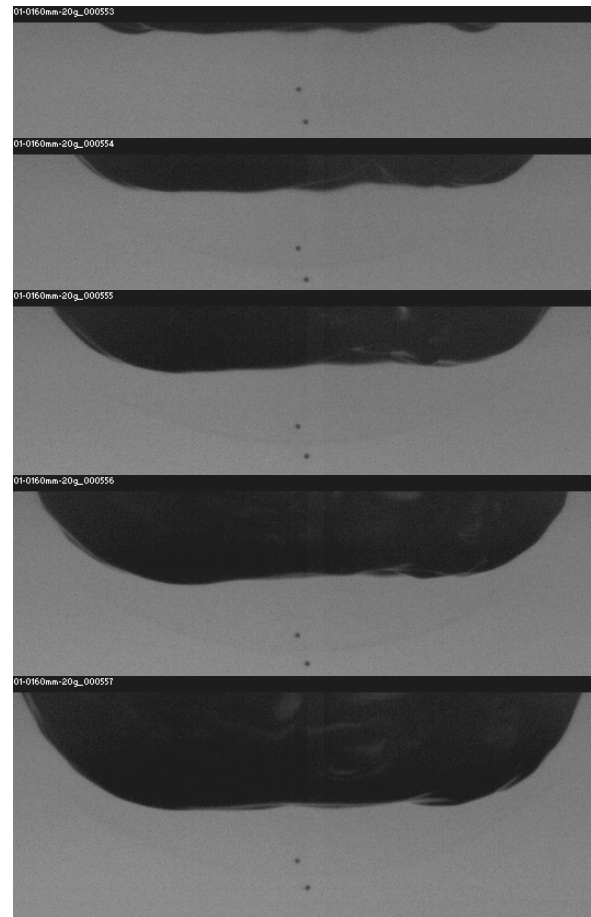

Figure 2. Sequence of successive image starting 1.67 ms after drop impact ($Fr = 174$, $We = 100$, $Re = 3463$, $t_c = 1.10$ at 3000 fps). A hemispherical bubble cloud can be seen between the positions of the two Thoroddsen bubbles.

The Oguz-Prosperetti bubbles are too small at the pixel resolution (12 µm) to be photographed and based on the limit of resolution, the maximum volume of the bubbles in the cloud is estimated at 200 µm^3.

Bubbles formed during cavity collapse

In this region, the cavity does not collapse spherically and the formation of non-linear capillary waves results in the base of the cavity being unable to rise fast enough before the sides of the cavity meet to form an entrapped bubble.

Primary entrapment

Figure 3 shows a sequence of primary bubble entrapment for different impact velocities. Over the range where primary bubble entrapment occurs, the Weber and Froude number varies by 1.7 times but the impact Reynolds number only varies by 1.3 times. As shown by Oguz and Prosperetti [6] the limits of primary bubble entrapment can be delineated by Fr-We relationships. Across the region, the shape of the cavity base prior to bubble entrapment changes quite dramatically, from a thin cylinder to a triangular shape. The bubble sizes in this region increases with Fr and We numbers until a steady bubble size is reached, in this case being an equivalent spherical diameter of 0.8 mm. In Figure 3D,

the bubble that is entrapped initially has a triangular shape, and the sharp tip retracts after bubble entrapment to form a liquid jet that penetrates downwards into the bubble. Figure 4 shows the change in bubble size with the *Fr* number, for drops formed by a 33G needle.
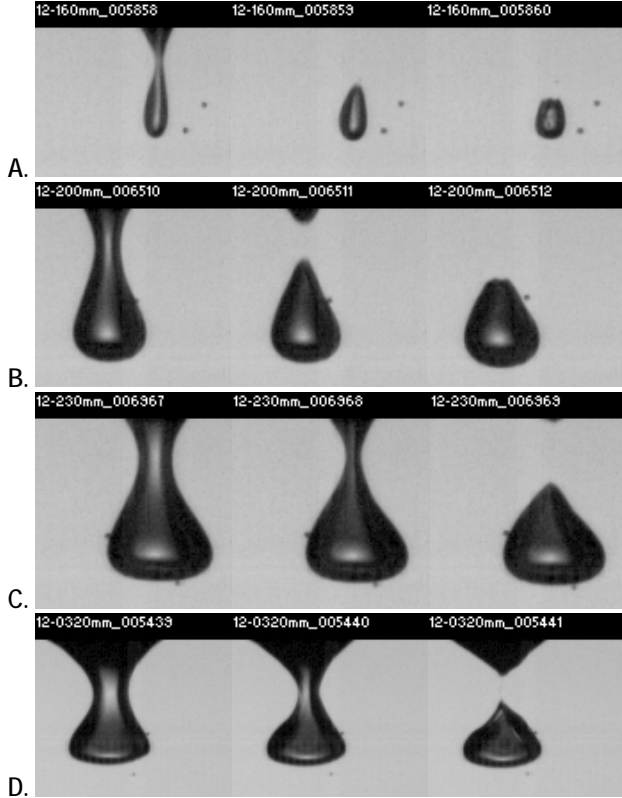

A.

B.

C.

D.

Figure 3. Set of four different primary bubble entrapment sequences from the beginning to the end of the regime. A. *d* = 2.13 mm, *U* = 2.02 m/s, *Fr* = 186, *We* = 114, *Re* = 3749. B. *d* = 2.16 mm, *U* = 2.16 m/s, *Fr* = 221, *We* = 137, *Re* = 4139. C. *d* = 2.14 mm, *U* = 2.28 m/s, *Fr* = 246, *We* = 152, *Re* = 4346. D. *d* = 2.15 mm, *U* = 2.62 m/s, *Fr* = 317, *We* = 193, *Re* = 5014.
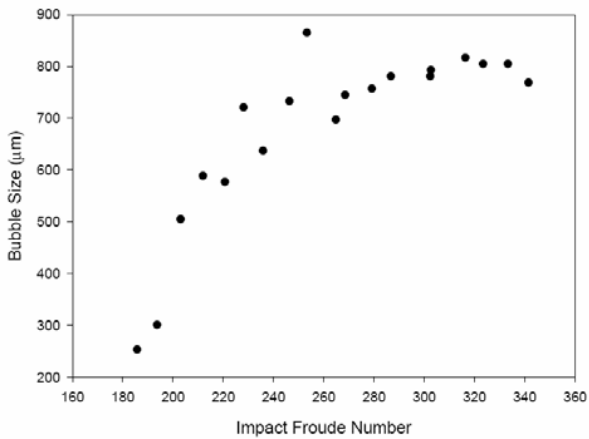

Figure 4. Size of bubbles formed in the primary entrapment region as a function of the impact Froude number. The drops were formed from a 33G needle.

As *Fr* is increased, the downward jet becomes stronger and may result in the entrapped bubble being split to form a bubble pair. Figure 5 shows the formation of a bubble pair. The region for entrapped bubble pair formation is fairly small, in this study, it occurred over the *Fr* of 332 to 343 for the drops from a 33G needle. This is a small region equivalent to a change in fall height of only 20 mm. This may be the reason why Rein [7] only

randomly observed this bubble pair as the *Fr* range for its production is rather narrow.
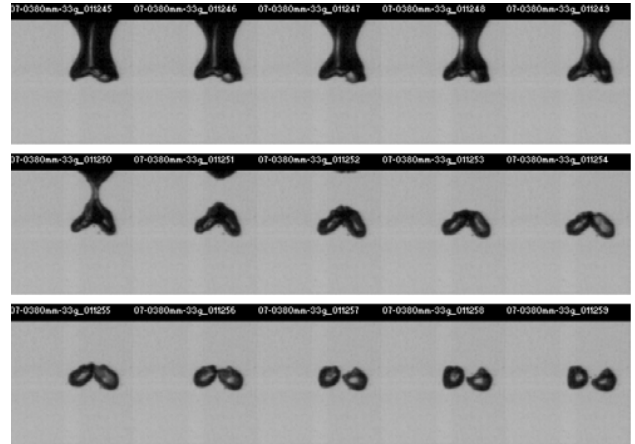

Figure 5. Formation of a bubble pair in the primary bubble entrapment region. *d* = 2.06 mm, *U* = 2.63 m/s, *Fr* = 343, *We* = 191, *Re* = 4826. At 40000 fps.
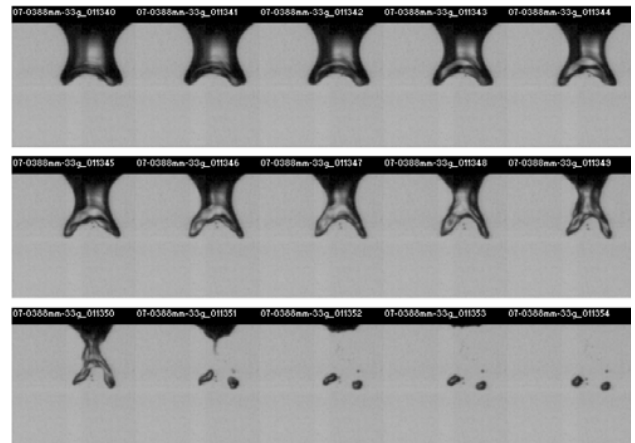
Secondary entrapment

Figure 6. Formation of secondary bubbles. *d* = 2.06 mm, *U* = 2.68 m/s, *Fr* = 356, *We* = 202, *Re* = 4904. At 40000 fps.
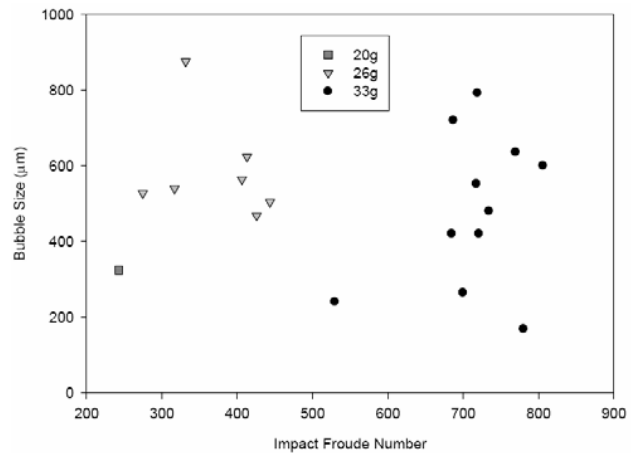

Figure 7. Size of bubbles formed in the secondary entrapment region as a function of the impact *Fr*. The *Fr* regime where the secondary entrapment occurs decreases with increasing impacting drop size.

At higher *Fr*, the base of the cavity collapses slower than the region above it. The base still spreads out and becomes unstable as surface tension is insufficient to bring the base back into a bubble. The edges of the base break off to form smaller bubbles

as shown in Figure 6. This has been classified as secondary bubble entrapment by Liow [4] as the mechanism is due to finger instability of the bubble base and is different from the primary bubble entrapment case. The number and size of the secondary bubbles formed is much more variable. Figure 7 shows that there is a range of bubble size for each impact.

Bubbles formed from thin film rupture with a floating drop

This occurs at very low Froude and Weber numbers drop impacts. The drops originate from the break-up of the jet formed from the initial impact of drops with much higher Froude numbers. The floating drops only partially coalesce and a smaller satellite drop is ejected. A coalescence cascade is formed as successive smaller drops repeat the same process.
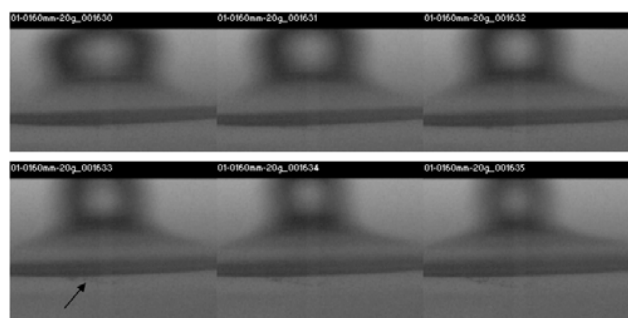
Floating drops – slow drainage

Figure 8. Bursting of a thin film beneath a floating drop at 3000 fps.

Figure 8 shows a 2 mm drop floating on the surface of the water. The drop comes from the break up of the jet formed for a 160 mm drop height impact of a 4 mm diameter drop. An air film separates the floating drop from the bulk liquid. The arrow shows the initial bursting of the air film and the last frame shows a cluster of small bubbles. The rupture of the air film results in the drop coalescing with the bulk fluid. It is found that the We for all the floating drops where drainage is slow is less than 6.

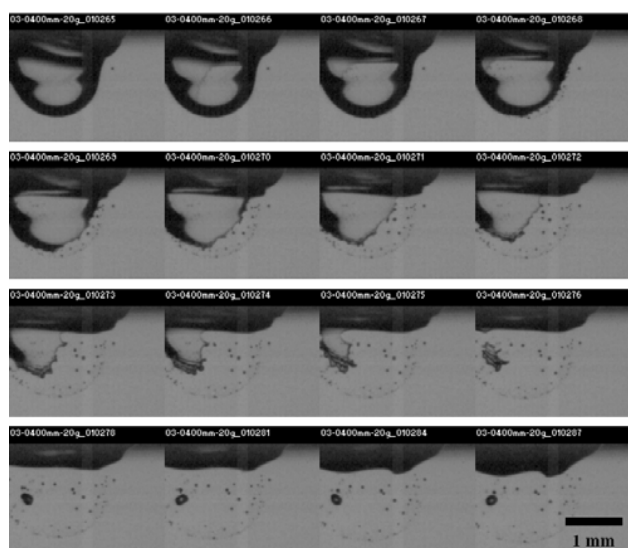### Floating drops – rapid expansion of air film (Mesler micro-bubbles)

Figure 9. Bursting of a thin film after stretching during drop impact at 27175 fps.

Figure 9 shows an image sequence of the air film break up. The air film is trapped by the impacting drop. The air film is initially pushed downwards until the momentum of the impacting drop is exhausted. Then the air film expands horizontally outwards thinning the air film until rupture occurs. The rupture occurs with a tear and then the air film rolls up with a spray of fine bubbles between 12 and 60 µm in diameter and a large bubble, 192 µm in diameter, from the rolled up air film. The film retraction has been measured at approximately 4 m/s. This rapid bursting was first reported by Esmailizadeh and Mesler [2]. The critical factor in inducing Mesler type micro-bubble formation is that the drop must contain enough energy to expand the air film to an unstable thickness.

Experiments have shown that the amount of fine bubbles increases with increasing impact velocity. Most of the micro-bubbles formed have been below the 12 µm, the resolution of the lens system used to photograph the sequence of events. We for the drops found to have a rapidly thinning lies between 6 and 20.

Conclusions

This study has shown that there are numerous mechanisms by which gas bubbles can be entrapped into a liquid during the splashing of a liquid drop. The entrapment of air in water is a crucial step in the aeration of water that keeps marine life vibrant as we know it. The study has covered drop impact Froude and Weber numbers les than 1000. All the different mechanisms identified for bubble formation were found for all the three different drop sizes used.

An area that has not been studies is the formation of large air bubbles due to the closing of the crown canopy during the impact of large raindrops at close to terminal velocities. Thus there remains a large region of Froude and Weber numbers to be investigated for gas bubbles formation from liquid drop impacts which may shed further light on the processes that sustain marine life.

References
[1] Blanchard, D. C. & Woodcock A. H. (1957). Bubble formation in the sea and its meteorological significance. *Tellus*, **9**, 1957, 150-158.
[2] Esmailizadeh, L. & Mesler R. Bubble entrainment with drops. *J. Coll. Int. Sci.*, **110**(2), 1985, 561-574.
[3] Franz, G. J. Splashes as sources of sound in liquids. *J. Acoust. Soc. Am.*, **31**(8), 1959, 1080-1096.
[4] Liow, J. L. Splash formation by spherical drops. *J. Fluid Mech.*, **427**, 2001, 73-105.
[5] Oguz, H. N. & Prosperetti A. Surface-tension effects in the contact of liquid surfaces. *J. Fluid Mech.*, **203**, 1989, 149-171.
[6] Oguz, H. N. and Prosperetti A. Bubble entrainment by the impact of drops on liquid surfaces. *J. Fluid Mech.*, **219**, 1990, 143-179.
[7] Pumphrey, H. C. & Crum L. A. Underwater sound produced by individual drop impacts and rainfall. *J. Acoust. Soc. Am.*, **85**(4), 1989, 1518-1526.
[8] Rein, M. The transitional regime between coalescing and splashing drops. *J. Fluid Mech.*, **306**, 1996, 145-165.
[9] Sigler, J. & Mesler R. The behaviour of the gas film formed upon drop impact with a liquid surface. *J. Coll. Int. Sci.*, **134**(2), 1990, 459-474.
[10] Thoroddsen, S. T., Etoh T. G. & Takehara K. Air entrapment under an impacting drop. *J. Fluid Mech.*, **478**, 2003, 125-134.